ADVANCED FUNCTIONAL MATERIALS
www.afm-journal.de

Materials Views
www.MaterialsViews.com

FULL PAPER

Self-Limited Nanocrystallization-Mediated Activation of Semiconductor Nanocrystal in an Amorphous Solid

*Shifeng Zhou, Chaoyu Li, Guang Yang, Gang Bi, Beibei Xu, Zhanglian Hong, Kiyotaka Miura, Kazuyuki Hirao, and Jianrong Qiu**

The construction of semiconductor nanocrystal (SNC)-based composites is of fundamental importance for various applications, including telecommunication, lasers, photovoltaics, and spintronics. The major challenges are the intentional insertion of dopants into SNCs for expanding their intrinsic functionalities and the scalable incorporation of activated SNCs into host free of hydroxyl and organic species for stabilizing and integrating their performances. An in situ approach is presented to couple the SNC doping and loading processes through self-limiting nanocrystallization of glassy phase, enabling one-step construction of fully transparent Ga_2O_3 SNC–glass nanocomposites. It is shown that the intentional introduction of various cation/anion impurities (e.g., F^-, In^{3+}, and Ni^{2+}) or their combinations into Ga_2O_3 SNCs can be realized by taking advantage of the viscous glass matrix to enhance the desorption barrier of impurity on the SNC surface and strengthen its tendency to incorporate into the SNC lattice. The composite can be rationally activated to show wavelength-tunable and broadband luminescence covering the spectral ranges of near ultraviolet, visible, and near-infrared wavebands. The approach is predicted to be general to other SNC materials for functional modulations and will be promising for scalable fabrication of novel SNC-based composites.

1. Introduction

A central theme in green photonics is the design and fabrication of optical materials with controlled optical properties and new functionalities. Semiconductor nanocrystals (SNCs) are a growing class of materials that have attracted considerable attention in photonics due to their unique tunable optical properties.[1–5] Impurity doping plays a crucial role in defining the optical properties of SNCs. For examples, the incorporation of active dopants such as Cu^+/Mn^{2+} into ZnSe and In^{3+} into Ga_2O_3 SNCs can effectively extend the luminescence waveband and simultaneously mitigate the toxicity problem of using cadmium and lead.[6–8] An intentional introduction of carriers into SNCs may also reduce the lasing threshold, thus greatly enhancing their optical behavior.[9,10] Despite great progress in doped SNC synthesis, nanodoping still remains a great challenge during the nanocrystallization process, as the host matrix on the nanoscale energetically drives the dopants towards the surface through the commonly assumed "intrinsic self-purification" mechanism.[11–14] On the other hand, for many photonic applications, preformed SNCs should be incorporated into inert media free of aqueous and organic solvents not only for prevention of optical loss caused by hydroxyl and organic species but also to improve the processability.[15] Herein, an effective one-step approach is reported to couple the SNC doping and loading processes through self-limiting nanocrystallization of glassy phase in a dry environment, making it possible to address the doping issue and simultaneously construct fully transparent SNC–glass nanocomposites with significant wavelength-tunable and broadband luminescence in the spectral ranges of near-ultraviolet, visible, and near-infrared wavebands.

2. Results and Discussion

Previous theoretical models and experimental facts have shown that the initial adsorption of impurities on the SNC surface is the underlying mechanism that controls doping.[16–18] Conceivably, the superior flowability of fluids in conventional solution or vapour crystallization process may greatly decrease the activation

---

Prof. S. F. Zhou, Prof. J. R. Qiu
State Key Laboratory of Luminescent Materials and Devices
Institute of Optical Communication Materials
South China University of Technology
Guangzhou, 510640, China
E-mail: qjr@scut.edu.cn

Prof. S. F. Zhou, C. Y. Li, B. B. Xu, Prof. Z. L. Hong, Prof. J. R. Qiu
State Key Laboratory of Silicon Materials
Department of Materials Science and Engineering
Zhejiang University
Hangzhou, 310027, China

Prof. G. Yang
Electronic Materials Research Laboratory
Key Laboratory of the Ministry of Education
and International Center for Dielectric Research
Xi'an Jiaotong University, Xi'an, 710049, China

Prof. G. Bi
School of Information and Electrical Engineering
City College, Zhejiang University
Hangzhou, 310015, China

Prof. K. Miura, Prof. K. Hirao
Department of Material Chemistry
Kyoto University
Nishikyo-ku, Kyoto, 615-8510, Japan

DOI: 10.1002/adfm.201300969

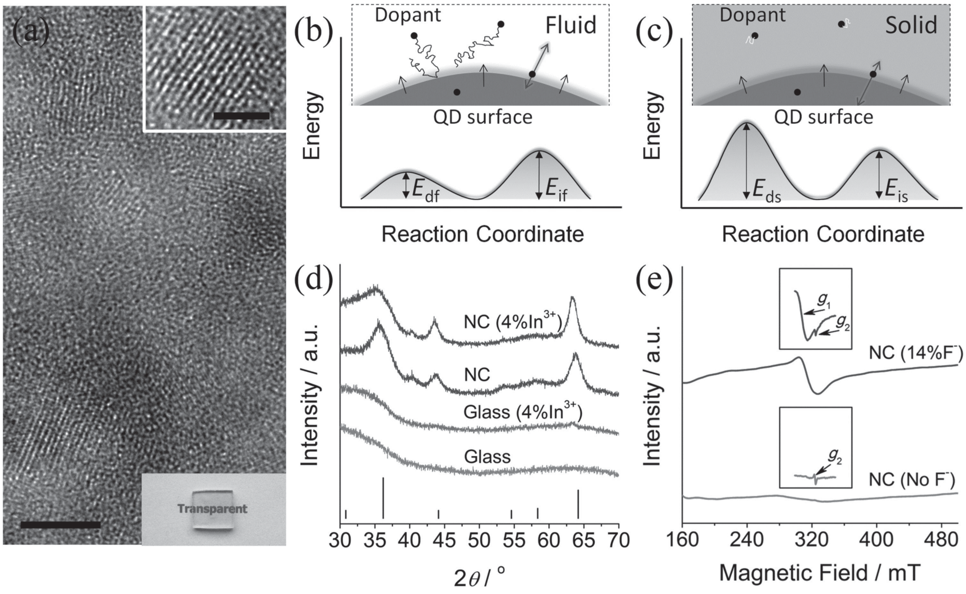

Figure 1. a) TEM image of a nanocrystallized sample embedded with Ga_2O_3:In^{3+}/F^- (scale bar = 4 nm). Insets: high-resolution TEM image showing well-defined lattice fringes of SNCs (scale bar = 2 nm); photograph indicating the high transparence of the obtained composite. b and c)Schematic presentations of dopant diffusion and the corresponding qualitative energetics in super-flowable fluid and viscous amorphous solid, respectively. E_{df}, E_{if}, E_{ds}, and E_{is} represent the activation barriers for dopant desorption and doping in flowable fluid and viscous amorphous solid, respectively. Black and white random curves indicate dopant diffusion traces. Black pieces and uni-directional arrows represent the surface of SNCs and their migration direction. Double arrows denote the balance between lattice incorporation and lattice ejection of dopants. d) XRD patterns of as-made glass and nanocrystallized samples (NCs) in the presence of 0 and 4 mol% In^{3+} dopant ions. e) ESR spectra of NCs in the presence of 0 and 14 mol% F^- dopant ions.

barrier for impurity desorption (E_{df} in **Figure 1**b), even making it lower than the activation barrier for impurity incorporation (E_{if} in Figure 1b). The resulting negative potential energy ($E_{df} - E_{if}$) may cause unstable adsorption of an impurity on the surface of nanocrystal and potentially amplify influence factors such as the shape and morphology of SNCs and surfactants, leading to the consequent failure in doping (the inset sketch in Figure 1b). This limitation invited consideration of the possibility of modulating the nonequilibrium adsorption–desorption kinetics of dopant for the purpose of rational doping. To this end, a scheme was devised to employ a viscous amorphous solid as the doping environment, taking advantage of the viscous matrix to suppress the migration of ions and facilitate the self-limited growth of nanocrystal. In contrast to the high-flow condition, the viscous environment is dense enough to remarkably enhance the desorption barrier of impurities (E_{ds} in Figure 1c), enabling it to surpass even the activation barrier for impurity incorporation (E_{is} in Figure 1c). This will be very helpful for strengthening the tendency of impurities to incorporate into the crystalline lattice during grain-boundary extension (the inset sketch in Figure 1c). We reason that this diffusion-limited process can be fully utilized for doping purposes based on a rational control over the structure and components of the glassy phase.

We initially succeeded in producing In^{3+}-doped metastable γ-Ga_2O_3 SNCs, which have recently attracted considerable scientific and technological interest.[8] In a typical experiment, we chose SiO_2 as the basic glass-forming oxide since it is highly inert and diverse functional units (e.g., Ga_2O_3 and In_2O_3) and other modifiers can be introduced to it. After melting the mixture of certain components at appropriate temperature, a highly transparent amorphous solid can be obtained. As a distinct advantage, the nanocrystallization tendency of a specific component in glassy phase can be determined based on a systematic valuation on the bond strength (B) and field strength (F). B- and F-values of the interested components were calculated and shown as follows: $B_{Ga\text{-}O}$ = 188 kJ mol^{-1}, $B_{In\text{-}O}$ = 180 kJ mol^{-1}, $B_{Si\text{-}O}$ = 443 kJ mol^{-1}, F_{Ga3+} = 0.77, F_{In3+} = 0.65, and F_{Si4+} = 1.54.[19] The stark contrast in structural features between –Ga–O–/–In–O– and –Si–O– units implies a great tendency to form local heterostructures in the glass phase and easily produce phase separation at the nanoscale. As anticipated, further heat-treatment of the amorphous solid results in the precipitation of γ-Ga_2O_3 SNCs with high crystallinity, as proved by transmission electron microscopy (TEM) (Figure 1a and Supporting Information Figure S1) and X-ray diffraction (XRD) patterns (Figure 1d). To demonstrate the success in In^{3+}-doping, we investigated the sample with a 4% doping level, which should result in a unit-cell volume expansion (ca. 8.65%). This is supported by the XRD data, which show that the diffraction peaks shift towards lower angle with the addition of In_2O_3. The observed value of the expansion of unit-cell (ca. 1.74 ± 0.09%) is smaller than that expected, which can be explained if some In^{3+} ions remain in the glassy phase. Importantly, we also observed that the full width at half-maximum of diffraction peaks did not show significant change with increasing heat-treatment temperature (Supporting Information, Figure S2), indicating a negligible change of the average crystallite size and the self-limiting nanocrystallization feature of Ga_2O_3 SNCs in glassy phase.

To further validate the scheme, we tested the possibility of intentionally introducing impurity ions with a sharp contrast in bond character from Ga_2O_3 SNCs. F^- was selected as the model dopant owing to its higher tendency to form ionic bonds in comparison with O^{2-} and the remaining difficulty in doping of it into oxide host through a colloidal chemical approach. We modified the mother glass system by adding a 5–15% (molar ratio) of fluorite (e.g., MgF_2). Electron spin resonance (ESR) was utilized to probe the extra electrons and the results are shown in Figure 1e. Notably, the F^--doped nanocrystallized sample presents a rather intense signal in the waveband region of 300–350 mT. The pinpoint scanning spectrum (the inset of Figure 1e) reveals the existence of two centers with $g_1 = 2.052$ and $g_2 = 2.001$. In contrast, the F^--free sample only shows a highly weak and sharp ESR signal with $g_2 = 2.001$, which can be assigned to the native non-bridging oxygen hole center of glass matrix.[20] Therefore, the signal with $g_1 = 2.052$ exceptionally observed in F^--doped sample is most likely related to the donor state induced by F^- incorporation in Ga_2O_3 SNCs. The ESR peak of F^--doped sample broadens and slightly shifts to low *g*-value in comparison with free electrons ($g = 2.0023$), indicating the strong interactions between dopants and highly localized feature of electrons, which are well consistent with the nature of electron donors in Ga_2O_3 SNCs.[21,22]

According to defect chemistry, substitutional replacement of O^{2-} with F^- may create a donor state in the semiconductor, thus potentially imparting new optical properties to SNCs. Interestingly, nanocrystallized samples doped with F^- show intense blue luminescence, which can be clearly observed with the naked eye (**Figure 2**a). Note that the F^--free sample only shows very weak emission and intense blue luminescence in F^--doped samples arises synchronously with the precipitation of Ga_2O_3, indicating the strong correlation between optical activity and F^- doping in Ga_2O_3 SNCs. Steady-state photoluminescence (PL) spectroscopy was employed to study the luminescence feature; the results are displayed in Figure 2a. Typically, PL spectra present broad emission bands with the maximum around 410–450 nm, which are very similar to the recombination transition of donor–acceptor pairs (DAP) in oxygen-deficient Ga_2O_3.[22] It is known that substitutional incorporation of F^- in Ga_2O_3 may generate a defect level in the bandgap and the observed blue luminescence can be assigned to the tunnel recombination involving a nearby DAP of F^x_O and $(V_O, V_{Ga})x$. According to the DAP model,[23] the energy of emitted light is determined by the defect state and bandgap of SNCs. Since In is chemically similar to Ga and the band gap of In_2O_3 ($E_g \approx 3.7$ eV) is smaller than that of Ga_2O_3 ($E_g \approx 4.9$ eV), we expected that a further introduction of In^{3+} into F^--activated Ga_2O_3 SNC would decrease its bandgap and thus facilitate the manipulation of light emissions. As anticipated, the PL can be continuously tuned from near ultra-violet to blue and even blue-green wavebands, based on the combined control of the crystallization temperature and co-doping with In^{3+} (Figure 2a). Importantly, we also succeeded in fabricating nanocrystallized samples into fibers which still kept the intense blue luminescence (Figure 2b), demonstrating the possibility of construction of fiber light sources. The fluorescence quantum yield of the nanocrystallized sample (660 °C) was estimated to be around 21.48%.

To highlight the unique feature of dopant activation through self-limiting nanocrystallization in the glassy phase, we made a detailed investigation on the PL peak energy dependence on the nanocrystallization temperature in F^- singly doped Ga_2O_3 SNCs and the results are shown in Figure 2c. Curiously, with the increased temperature, PL presents an initial red-shift, which is similar to our previous investigation, and a subsequent blue-shift, that is an entirely different scenario from the case for the Ga_2O_3 SNCs obtained by solution crystallization method where only a monotonic blue-shift occurs.[22,24] In consideration of the large effective mass of electrons ($m_e \approx 0.34m_0$) and tight exciton binding, the quantum confinement in Ga_2O_3 is negligible, as has been proved experimentally.[8,22,25] Thus, it is more reasonable to ascribe the emission shift to the coulombic interaction change which can be described by the equation $E_C = e^2/4\pi\varepsilon R$, where ε is the low-frequency dielectric constant and R is the DAP separation distance.[23] Thus, the coulombic interaction has a DAP separation (R)-dependent property and for Ga_2O_3 SNCs with tiny size, the coulombic interaction can be expected to be especially strong as a consequence of high concentration donors in rather limited domain volumes (Stage A in Figure 2c). According to a Tamann classic diagram, at relatively low crystal growth temperature, a slight enhancement of thermal treatment may lead to a notable increase in the nanocrystal size while the moderate growth of donor quantity is maintained.[26] So the initial red-shift of emission can be associated with the reduced volume concentration of donor and the resulting increase in the DAP separation distance (Stage B in Figure 2c). However, further increase in temperature depresses the growth rate dramatically due to the formation of a Ga-depletion shell around crystallites. Indeed, Höche's results have experimentally shown the existence of unique interface between crystal and glass matrix which is probably rich in matrix components such as Si and can act

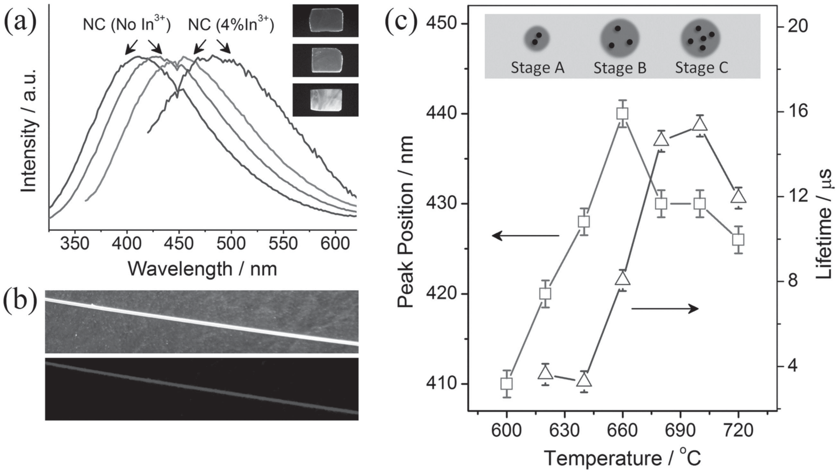

Figure 2. a) PL spectra of nanocrystallized samples (NC) embedded with $Ga_2O_3:F^-$ and $Ga_2O_3:In^{3+}/F^-$ (inset: photographs of nanocrystallized samples qualitatively illustrating the luminescence intensity. b) Photographs of the fabricated fiber (ca. 400 μm in diameter) under daylight and UV light. c) Peak position and decay lifetime of visible luminescence versus nanocrystallization temperature.

as a strong diffusion barrier.[27] As a typical glass component, F is also expected to accumulate in the shell region, ensuring its continuous incorporation into nanocrystals. As a result, Ga_2O_3 SNCs tend to have increased donor concentration and shorted DAP separation distance, leading to the blue-shift of luminescence band again (Stage C in Figure 2c). In addition to the improved ability in control of doping level, we also found that the luminescence performance of SNCs can be simultaneously enhanced through self-limiting nanocrystallization. Figure 2c also shows the crystallization temperature dependent decay lifetime and it is significantly to note that by increasing the crystallization temperature the emission lifetime at 430 nm can be greatly extended from 3.28 µs (at 640 °C) to 15.33 µs (at 700 °C), which is much longer than the Ga_2O_3 SNCs prepared by solution crystallization method (ca. 5 µs).[22] The decay curves are provided in the Supporting Information (Figure S3).

In a further set of experiments, we tried to introduce transition-metal ions (e.g., Ni^{2+}) into Ga_2O_3 SNCs based on the proposed strategy and more significantly, to demonstrate the possibility of optical property fine-tuning in a multiple doping system. **Figure 3**a shows the absorption spectra and photographs of mother glass and nanocrystallized samples doped with Ni^{2+}, Ni^{2+}/In^{3+}, Ni^{2+}/F^-, and $Ni^{2+}/F^-/In^{3+}$. In glass samples, three absorption bands at ca. 440, 870, and 1760 nm can be assigned, respectively, to the transitions of $^3E'(F) \rightarrow {}^3E''(F)$, $^3E'(F) \rightarrow {}^3A'_2(F)$, and $^3E'(F) \rightarrow {}^3A'_2(P)$ of the trigonal bipyramid fivefold and tetrahedral Ni^{2+}.[28] The precipitation of Ga_2O_3 SNCs leads to a drastic change in the appearance and absorption characteristic of all four samples. The newly appeared absorption bands at ca. 600 and 1010 nm correspond exactly to the $^3A_2(F) \rightarrow {}^3T_1(F)$ and $^3A_2(F) \rightarrow {}^3T_2(F)$ electronic transitions of octahedral Ni^{2+}.[29–31] We performed calculations on the electronic transitions of octahedral Ni^{2+} by using Tanabe-Sugano theory.[32] It was found that the theoretical electronic transitions are in good agreement with the experimentally observed absorption bands (Supporting Information, Table S1), indicating the origin of absorption variation associated with the geometrical change of Ni^{2+}. Moreover, a direct examination on the Ni M_{23} edge at ca. 67 eV by using electron energy-loss spectroscopy (EELS) shows that Ni^{2+} ions are preferentially rich in the Ga_2O_3 SNCs (Figure 3b). Taken together, these results strongly suggest that Ni^{2+} selectively

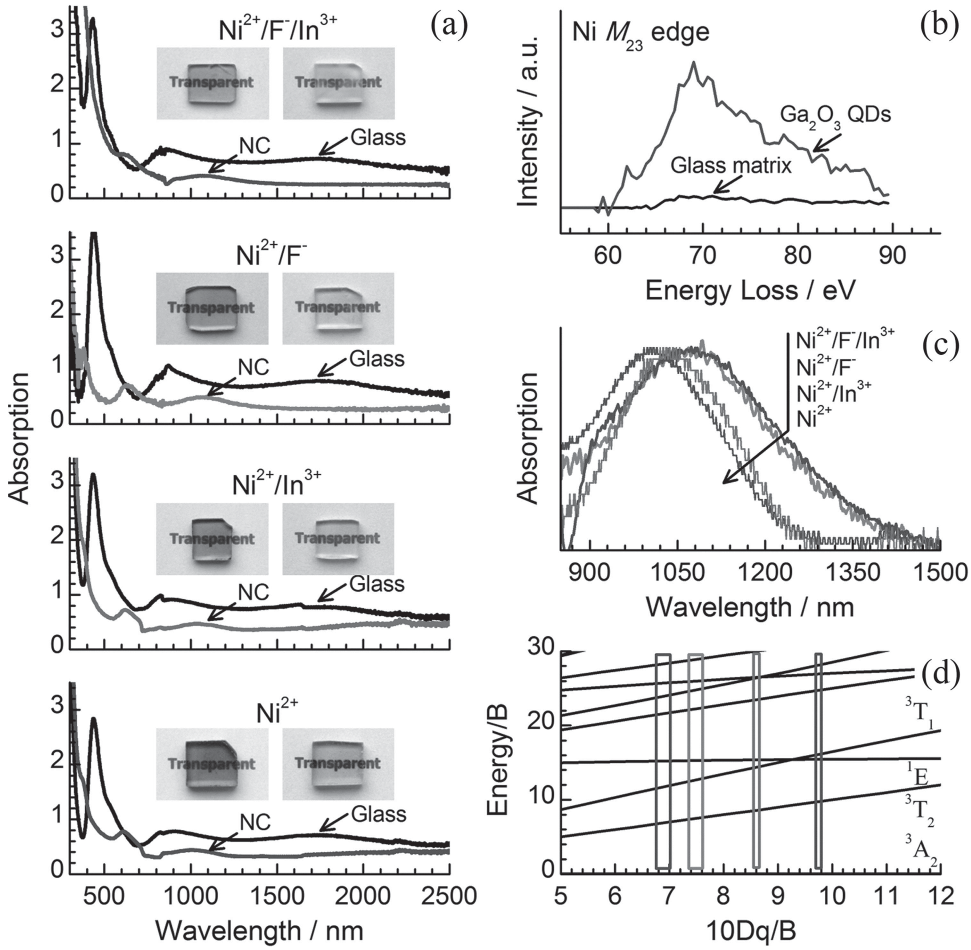

Figure 3. a) Absorption spectra of as-made glass and nanocrystallized samples (NC) embedded with Ga_2O_3:Ni^{2+}, Ga_2O_3:Ni^{2+}/In^{3+}, Ga_2O_3:Ni^{2+}/F^-, and Ga_2O_3:$Ni^{2+}/F^-/In^{3+}$. Inset: photographs of as-made glass (left) and nanocrystallized glass samples (right). b) EELS spectra of the Ni M_{23} edge in crystalline and glass regions. A heavily doped sample (2 mol% NiO) was used for analysis. c) Enlarged and normalized absorption spectra of nanocrystallized samples in the 850–1500 nm wavelength region. d) Ligand field energy level diagram for d^8 ions, in which the marked squares indicate the crystal field of Ni^{2+} in the nanocrystallized samples embedded with Ga_2O_3:Ni^{2+}, Ga_2O_3:Ni^{2+}/In^{3+}, Ga_2O_3:Ni^{2+}/F^-, and Ga_2O_3:$Ni^{2+}/F^-/In^{3+}$ (from right to left).

incorporates into Ga_2O_3 SNCs through substitution of octahedral Ga^{3+}. Significantly, a close inspection of the characteristic absorption band of Ni^{2+} in the 900–1200 nm wavelength region (corresponding to $^3A_2(F) \rightarrow {}^3T_2(F)$ transition) indicates a unique doping-dependent absorption feature (Figure 3c). Selective incorporation of In^{3+}, F^-, or In^{3+}/F^- combination into Ni^{2+}-doped nanocrystallized sample shifts the absorption band of Ni^{2+} to longer wavelengths with increased extent. Furthermore, a prominent broadening of absorption band was also observed in the F^--containing system. From the electronic absorption spectra, the ligand-field states of octahedral Ni^{2+} inside the SNCs can be calculated and the crystal field strength (Dq) values of Ni^{2+} are estimated to be around 993.0, 965.3, 934.6, and 921.7 cm^{-1} in the Ni^{2+}-, Ni^{2+}/In^{3+}-, Ni^{2+}/F^--, and $Ni^{2+}/F^-/In^{3+}$-doped nanocrystallized samples, respectively. Figure 3d gives an overview of the electronic energy level diagram for the d^8 electron configuration in the absence of spin-orbit coupling and the marked squares represent the locations of energy levels of Ni^{2+} in single-dopant (Ni^{2+}), two-component dopant (Ni^{2+}/In^{3+} and Ni^{2+}/F^-), and three-component dopant ($Ni^{2+}/F^-/In^{3+}$) systems. The results clearly show that the electron structure of Ni^{2+} can be rationally tuned by utilization of synergy effect between co-dopants. The strategy has not been previously reported partially due to the notorious difficulty in controllable incorporation of multiple dopants into strongly confined SNCs based on the conventional method.

To further clarify the effect of co-doping on the electronic structure of Ni^{2+}, we performed first-principles calculations based on the density functional theory (DFT) for the local structure of Ga_2O_3 SNCs. γ-Ga_2O_3 belongs to the defect spinel structural family (cubic, space group $Fd\bar{3}m$) in which Ga^{3+} ions occupy both octahedral and tetrahedral sites (**Figure 4**a,c). As shown in Figure 4d, DFT calculations show that the substitutional incorporation of In^{3+} in Ga_2O_3 perturbs lattice perfection, resulting in the prominent lattice expansion with the average cation–anion distance increasing from 2.031 to 2.441 Å and a slight fluctuation of bond angle (ca. 1.677°); this is consistent with our experimental observations showing that doping of In^{3+} shifts the XRD peaks to lower diffraction angle (Figure 1d). In contrast, replacement of O^{2-} by F^- only leads to a slight decrease of average bond-length to ca. 1.967 Å (Figure 4e), which should be expected in view of their similar ion radii (r_{O2-} = 1.40 Å; r_{F-} = 1.33 Å). Notably, the calculation results indicate the occurrence of profound ligand distortion with the average bond angle change estimated to be around 6.495° after incorporation of F^- (Figure 4e), most probably resulting from the significant electronegativity (χ) difference between O (χ = 3.44) and F (χ = 4). According to ligand field theory, the splitting of $3d$ orbital energy levels obeys the "centre of gravity" with the three t_{2g} orbitals being lowered by $4Dq$ and two e_g orbitals raised by $6Dq$ (Figure 4b). In a regular octahedral environment the total energy separation ($10Dq$) can be derived from the following relation:

$$10\,Dq = Q\langle r^4\rangle / R^5 \tag{1}$$

here, $\langle r^4\rangle$ is the mean value of the fourth power of the radial distance of a $3d$ orbital from the nucleus, R represents metal–ligand distance and Q is a constant.[33,34] Therefore, the decrease of the Dq of Ni^{2+} after In^{3+} incorporation (Figure 3d) primarily originated from the prominent increase of lattice parameters and bond-lengths in the host Ga_2O_3 SNCs. In addition to interatomic distance, another factor that greatly contributes to the crystal field splitting is the symmetry of ligand. Indeed, previous calculations have shown that regular octahedral symmetry generates the strongest crystal field and Dq values in octahedral, tetrahedral, body-centred cubic, and dodecahedral coordinations can be summarized as:[35]

$$Dq_o : Dq_c : Dq_d : Dq_t = 1 : -8/9 : -1/2 : -4/9 \tag{2}$$

Thus the distortion of coordination polyhedron after F^--doping can be expected to show the similar effect as symmetry change, leading to the pronounced decrease in crystal field splitting of Ni^{2+}. This supposition can be further experimentally verified by the spectral shift of ZnSe:Cu during the growth of the outer shell, which was ascribed to the symmetry increase.[6]

The success in engineering the electronic structure of a special activator by co-doping suggests an opportunity for manipulating radiative electron transition and the subsequent photon output. Interestingly, nanocrystallized samples show intense near-infrared luminescence from 1100 to 1700 nm upon excitation at 808 or 980 nm (**Figure 5**a). The luminescence can be attributed to the $^3T_2(F) \rightarrow {}^3A_2(F)$ radiative transition of octahedral Ni^{2+}. In contrast, the as-made glass does not show any emission, mainly owing to the thermally activated energy migration through $^3A'_2(P) \rightarrow {}^3E'(F)$ non-radiative transition of low crystal field Ni^{2+}. It should be pointed out that this undesired electronic transition of Ni^{2+} in glass totally vanished in nanocrystallized samples (Supporting Information, Figure S4), reflecting the capability to

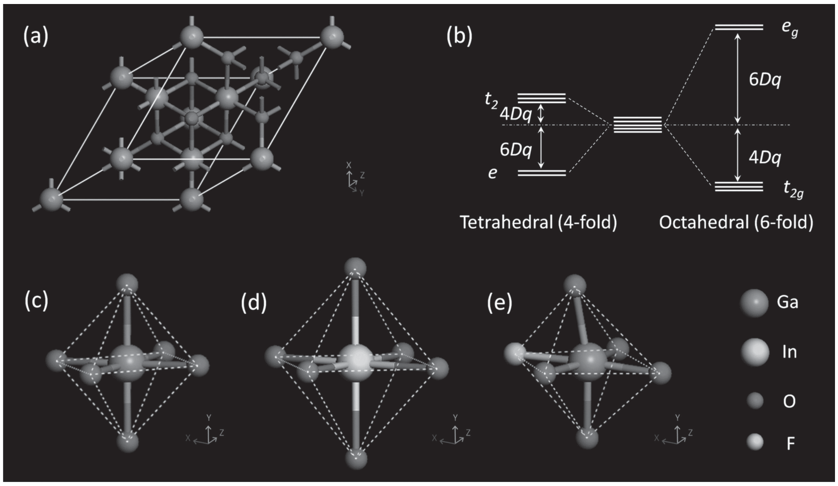

Figure 4. a) Crystal structure of γ-Ga_2O_3. b) Crystal field splitting of $3d$ orbitals of Ni^{2+} in tetrahedral and octahedral coordinations. c) Configurations of regular [GaO_6] octahedron. d and e) DFT calculation results showing the change of octahedron after substitutional incorporation of In^{3+} and F^-.

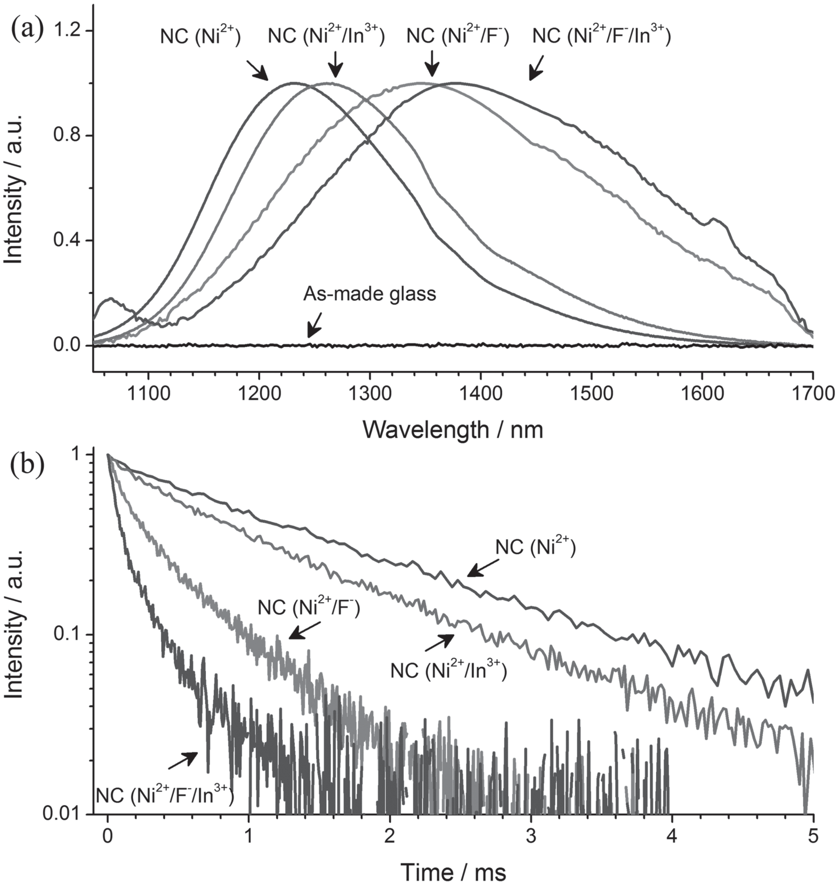

Figure 5. Room-temperature emission spectra (a) and fluorescence decay curves (b) of nanocrystallized samples embedded with Ga_2O_3:Ni^{2+}, Ga_2O_3:Ni^{2+}/In^{3+}, Ga_2O_3:Ni^{2+}/F^-, and Ga_2O_3:$Ni^{2+}/F^-/In^{3+}$. The emission spectrum of as-made glass doped with Ni^{2+} is also shown for comparison.

completely block the non-radiative relaxation channel and additionally confirming the added possibility to achieve high doping efficiency through in situ self-limiting nanocrystallization. Importantly, the emission can be continuously tuned from 1200, 1250, 1350, to 1400 nm, and, surprisingly, the decay rate can also be tuned (Figure 5b) by rational doping of Ni^{2+}, Ni^{2+}/In^{3+}, Ni^{2+}/F^-, and $Ni^{2+}/F^-/In^{3+}$. The lifetimes of the longest component for Ni^{2+}-, Ni^{2+}/In^{3+}-, Ni^{2+}/F^-,- and $Ni^{2+}/F^-/In^{3+}$-doped nanocrystallized samples were estimated to be around 1537, 1351, 639, and 332 μs, respectively (Supporting Information, Figure S5–8). The observed optical properties in these nanocrystallized samples are especially interesting since they have provided the first observation of effective light-emitting management from transition-metal-ion activated SNCs in the whole telecommunication low-loss window (1200–1600 nm) which is simply triggered by the optically inactive co-dopants. To explain the unique tunable and ultra-broadband luminescence properties induced by doping, we re-investigated the absorption and luminescence spectra. From Figure 3c and 5a, it can be noticed that the co-doping-induced change in the trend of luminescence features is perfectly in accord with that of absorption, indicating their same origins associated with the ligand field effect. As shown in Figure 3d, the fluctuation of *Dq* may shift the locations of the energy levels of Ni^{2+}, leading to a controllable energy gap between $^3T_2(F)$ and $^3A_2(F)$ levels and tunable luminescence with a certain Stokes' shift. The strong correlation between decay rate (τ) and *Dq* can be considered in the context of Mott and Gurney model.[36,37] Generally, the decay of Ni^{2+} is mainly dominated by the multiphonon relaxation effect and the process can be described by a Arrhenius factor related to the occupation probability of the electrons in the vibrational excited state, given by:

$$\tau = A \exp\left(-\Delta E / kT\right) \tag{3}$$

where A is a constant, k is the Boltzmann constant, T is the temperature, and ΔE is the activation energy. That is, the luminescence decay rate is affected by ΔE, which equals to the energy difference between the ground state of the $^3T_2(F)$ level and the crossover of the potential energy surfaces of the levels of $^3T_2(F)$ and $^3A_2(F)$, as shown in the generalized single configurational coordinate diagram (Supporting Information, Figure S9). We call attention to the fact that the increase of *Dq* parameter may raise the position of $^3T_2(F)$ parabola while the ground $^3A_2(F)$ parabola keeps no change, thus driving an enhancement of ΔE and extension of decay lifetime. For this reason, the changes of the decay lifetime ($\tau_{Ni^{2+}} > \tau_{Ni^{2+}/In^{3+}} > \tau_{Ni^{2+}/F^-} > \tau_{Ni^{2+}/F^-/In^{3+}}$) in nanocrystallized samples were found to mirror the order of crystal field strength ($Dq_{Ni^{2+}} > Dq_{Ni^{2+}/In^{3+}} > Dq_{Ni^{2+}/F^-} > Dq_{Ni^{2+}/F^-/In^{3+}}$).

Furthermore, it is possible that the distortion of local structure may induce formation of mixed Ni^{2+} environments with different *Dq*. Consequently, an inhomogeneous line-shape broadening in nanocrystallized samples can be expected. Indeed, a notable spectral broadening from 200 to 350 nm can be exclusively observed in F^- -containing samples (Figure 5a), mainly originating from the profound local ligand distortion after F^- incorporation (Figure 4e). It was found that the near-infrared fluorescence decay curves of F^--doped samples cannot be fitted to a single first-order exponential equation, giving a clear indication for the existence of multiple active centers (Supporting Information, Figure S7,S8). In addition, photoluminescence excitation (PLE) and time-resolved PL measurements also show the shift of excitation bands and the existence of different luminescence decay profiles by changing the detection wavelength (Supporting Information Figure S10,S11), which additionally demonstrates the site-to-site variation of Ni^{2+} centers.

As is well-known, the most important spectroscopic features that make doped materials relevant for photonic applications are bandwidth, lifetime, and stimulated-emission cross-section. We summarized the optical properties of some commercial gain materials for tunable lasers, as shown in **Table 1**. It is exciting

Table 1. Comparison of optical properties for transition-metal ions doped materials (glasses and crystals) and Ni^{2+}-doped materials (glasses, crystals, and nanostructures) with Ni^{2+}-doped nanocrystallized samples.

Material	Emission [cm^{-1}]	Bandwidth [cm^{-1}]	Lifetime [μs]	Reference
$LiInGeO_4$: Cr^{4+}	ca. 8333	ca. 1890	ca. 7.3	[38]
Glass:Cr^{4+}	ca. 7692	ca. 1350	–	[39]
$BaSO_4$:Mn^{6+}	ca. 9090	ca. 1900	ca. 0.65	[40]
Chalcogenide glass:Ni^{2+}	ca. 7407	ca. 2083	ca. 40	[41]
$Al_{18}B_4O_{33}$ nanorod:Ni^{2+}	ca. 7692	ca. 1505	<1	[42]
$MgAl_2O_4$:Ni^{2+}	ca. 8474	ca. 1046	ca. 400	[43]
Nanocrystallized glass:Ni^{2+}	ca. 8333	ca. 1561	665	[37]
Nanocrystallized glass:Ni^{2+}	7142–8333	1350–1925	332–1537	This work

that the luminescence properties of the obtained nanocrystallized composites are superior to that of Ni^{2+}-doped chalcogenide glass, nanorods or other transition-metal-ion doped materials, and even comparable to Ni^{2+}-doped crystal. The notable extension in bandwidth and decay lifetime is believed to benefit from the effective doping strategy mediated by self-limiting nanocrystallization and the excellent physical properties of Ga_2O_3, such as large bandgap and moderate cutoff phonon energy (ca. 760 cm^{-1}) which favour the suppression of thermal-quenching effects. In addition, the luminescence intensity of samples can be enhanced after co-doping with other transition metal ions such as Cr^{3+} (Supporting Information, Figure S12) with the fluorescence quantum yield estimated to be around 7.65%.[44,45] Furthermore, the dry process for nanocrystallization can efficiently eliminate the optical loss caused by hydroxyl and organic species. Obviously, this local structure engineering in amorphous solid may enable a new opportunity to fabricate novel composite broadband gain materials which are highly attractive for applications in high-resolution confocal microscopy, medical tomography, and tunable lasers.[46–48] As an added benefit, a profound broadened emission spectrum observed here is also highly beneficial for minimizing signal cross-saturation and cross talk in modern super-high-capacity information transmission system.[49,50]

3. Conclusions

We have presented a robust approach for in situ activation of SNCs and one-step fabrication of activated SNC–glass composites via self-limiting nanocrystallization of the amorphous phase. This protocol has proven to be effective for intentionally introducing dopants into SNCs. It also offers the possibility of precisely manipulating photon emission of SNCs to cover the ultra-violet, visible, and near-infrared spectral ranges through simply tuning inert co-dopants, which is in stark contrast to previous methods that require careful control over the host materials and luminescence centers.[24,34,51–54] Thus it provides an alternative way to construct tunable light sources and simultaneously mitigate the toxicity problems of using Cd/Pb species associated with conventional methods. Furthermore, we note that this strategy should be general to other oxide SNCs (e.g., ZnO and SnO_2) and even non-oxide candidates (e.g., ZnS and ZnSe) by using various dopants (e.g., Cu^{2+} and Mn^{2+}) in consideration of the moderate field strength of Zn and Sn ($F_{Zn2+} = 0.52$; $F_{Sn2+} = 0.41$), pointing to future opportunities in electrical and magnetic properties control. The unique dopant activation scheme is also expected to operate in multi-component SNCs through rational combination of various local structure units and systematic analysis of their ordering tendency.

4. Experimental Section

Material Synthesis: The procedure for fabrication of transparent Ga_2O_3 SNCs-glass composites was designed based on the collecting detailed data on the standard phase diagram and experimental results about glass-forming property of the SiO_2–Ga_2O_3–Na_2O system, specifically investigating the composition dependent stability of glass phase, as well as the effects of heat-treatment temperature and duration on precipitation of Ga_2O_3 SNCs inside glass phase without serious loss of optical transparency. For In^{3+} and F^- singly doped and In^{3+}/F^- co-doped samples, the synthesis starts from the above ternary system, with the addition of Al_2O_3, MgO, MgF_2, and In_2O_3 to tune the linking properties of the glass network and simultaneously for doping purpose. The compositions of the mother glass were optimized to be $SiO_2/Ga_2O_3/Al_2O_3/Na_2O/MgO/In_2O_3$ = 56.5:19.5:6.5:7:10.5:2 (In^{3+} doped), $SiO_2/Ga_2O_3/Na_2O/MgF_2$ = 51:20:15:14 (F^- doped) and $SiO_2/Ga_2O_3/Na_2O/MgF_2/In_2O_3$ = 51:20:15:14:2 (In^{3+}/F^- co-doped) (molar basis). For Ni^{2+}-doping, NiO was selected as source material and the doping concentration was set to 0.15 mol%. Detailed experimental procedures can be found in Ceccato et al.[55] In a typical synthesis, about 20 g of raw materials were mixed thoroughly and melted in a covered corundum crucible at temperature range from 1500 to 1650 °C for 30 min, depending on the composition of the sample. The homogenized melt was then quenched into a preheated brass mold to form the mother glass. Thermal analysis was performed on the mother glass and the results were used to guide the design of procedure for in situ thermal activation of Ga_2O_3 SNCs. Highly transparent Ga_2O_3 SNC–glass composites were successfully obtained by optimization of related parameters, including temperature and duration. Before optical characterization, samples were cut into pieces of about 10 × 10 × 1.5 mm^3 and polished carefully.

Material Characterization: The thermal properties of mother glass, including the glass-transition and crystallization temperatures, were studied with differential thermal analysis at a heating rate of 10 K min^{-1}. The crystalline phases precipitated inside the composite were identified by X-ray diffraction by using Cu/Kα radiation. Microstructure and microanalysis were performed using a JEOL ARM200F, equipped with a Gatan Enfina electron energy-loss spectrometer, operating at a voltage of 200 kV. Absorption spectra were recorded using a UV-3150 UV-vis-NIR spectrophotometer (Shimadzu Corp., Japan). PL spectra, PLE spectra, and the fluorescence decay curves in both the visible and infrared wavelength regions were measured using a FLS920 fluorescence spectrophotometer (Edinburgh Instrument Ltd., UK). The fluorescence quantum yield was measured by using a FLS920 fluorescence spectrophotometer (Edinburgh Instrument Ltd., UK) equipped with a barium sulfate-coated integrating sphere. Every spectrum was scanned three times to eliminate noise. The quantum yield (QY) was calculated by the following equation:

$$\eta = \frac{\int L_S}{\int E_R - \int E_S} \tag{4}$$

where L_S is the luminescence spectrum, and E_R and E_S are the spectra of excitation light without and with the sample, respectively.[56] All of the spectra were measured inside the integrating sphere and scanned three times to eliminate noise.

Supporting Information

Supporting Information is available from the Wiley Online Library or from the author.

Acknowledgements

This work was financially supported by the National Natural Science Foundation of China (grant nos. 51132004, 51072054, and 51102209), the National Basic Research Program of China (2011CB808100), the Fundamental Research Funds for the Central Universities, and the Open Fund of the State Key Laboratory of Modern Optical Instrumentation (Zhejiang University). G.B. acknowledges the financial support from National Natural Science Foundation of China (no. 61275108) and Natural Science Foundation of Zhejiang Province in China (no. Y111049).

Received: March 18, 2013

[1] S. Coe, W. Woo, M. Bawendi, V. Bulović, *Nature* **2002**, *420*, 800.
[2] E. H. Sargent, *Adv. Mater.* **2005**, *17*, 515.
[3] T. Mokari, M. Zhang, P. Yang, *J. Am. Chem. Soc.* **2007**, *129*, 9864.
[4] V. I. Klimov, S. A. Ivanov, J. Nanda, M. Achermann, I. Bezel, J. A. McGuire, A. Piryatinski, *Nature* **2007**, *447*, 441.
[5] C. Dang, J. Lee, C. Breen, J. S. Steckel, S. Coe-Sullivan, A. Nurmikko, *Nat. Nanotechnol.* **2012**, *7*, 335.
[6] N. Pradhan, D. Goorskey, J. Thessing, X. Peng, *J. Am. Chem. Soc.* **2005**, *127*, 17586.
[7] S. K. Panda, S. G. Hickey, H. V. Demir, A. Eychmüller, *Angew. Chem., Int. Ed.* **2011**, *50*, 4432.
[8] S. S. Farvid, T. Wang, P. V. Radovanovic, *J. Am. Chem. Soc.* **2011**, *133*, 6711.
[9] C. Wang, B. L. Wehrenberg, C. Y. Woo, P. Guyot-Sionnest, *J. Phys. Chem. B* **2004**, *108*, 9027.
[10] D. J. Norris, A. L. Efros, S. C. Erwin, *Science* **2008**, *319*, 1776.
[11] S. C. Erwin, L. Zu, M. I. Haftel, A. L. Efros, T. A. Kennedy, D. J. Norris, *Nature* **2005**, *436*, 91.
[12] G. M. Dalpian, J. R. Chelikowsky, *Phys. Rev. Lett.* **2006**, *96*, 226802.
[13] T. Chan, A. T. Zayak, G. M. Dalpian, J. R. Chelikowsky, *Phys. Rev. Lett.* **2009**, *102*, 025901.
[14] D. Mocatta, G. Cohen, J. Schattner, O. Millo, E. Rabani, U. Banin, *Science* **2011**, *332*, 77.
[15] C. Meng, Y. Xiao, P. Wang, L. Zhang, Y. Liu, L. Tong, *Adv. Mater.* **2011**, *23*, 3770.
[16] K. G. Stamplecoskie, L. Ju, S. S. Farvid, P. V. Radovanovic, *Nano Lett.* **2008**, *8*, 2674.
[17] M. Du, S. C. Erwin, A. L. Efros, *Nano Lett.* **2008**, *8*, 2878.
[18] D. Chen, R. Viswanatha, G. L. Ong, R. Xie, M. Balasubramaninan, X. Peng, *J. Am. Chem. Soc.* **2009**, *131*, 9333.
[19] W. D. Kingery, H. K. Bowen, D. R. Uhlmann, *Introduction to Ceramics*, Wiley-Interscience, John Wiley & Sons, New York **1975**.
[20] L. Skuja, *J. Non-Cryst. Solids* **1998**, *239*, 16.
[21] R. Wang, A. W. Sleight, D. Cleary, *Chem. Mater.* **1996**, *8*, 433.
[22] T. Wang, S. S. Farvid, M. Abulikemu, P. V. Radovanovic, *J. Am. Chem. Soc.* **2010**, *132*, 9250.
[23] D. G. Thomas, J. J. Hopfield, W. M. Augustyniak, *Phys. Rev. B* **1965**, *140*, A202.
[24] S. Zhou, N. Jiang, K. Miura, S. Tanabe, M. Shimizu, M. Sakakura, Y. Shimotsuma, M. Nishi, J. Qiu, K. Hirao, *J. Am. Chem. Soc.* **2010**, *132*, 17945.
[25] H. He, R. Orlando, M. A. Blanco, R. Pandey, E. Amzallag, I. Baraille, M. Rérat, *Phys. Rev. B* **2006**, *74*, 195123.
[26] G. H. Beall, L. R. Pinckney, *J. Am. Ceram. Soc.* **1999**, *82*, 5.
[27] S. Bhattacharyya, C. Bocker, T. Heil, J. R. Jinschek, T. Höche, C. Rüssel, H. Kohl, *Nano Lett.* **2009**, *9*, 2493.
[28] L. Galoisy, G. Calas, *Geochim. Cosmochim. Acta* **1993**, *57*, 3613.
[29] R. Moncorgé, T. Benyattou, *Phys. Rev. B* **1988**, *37*, 9186.
[30] B. N. Samson, L. R. Pinckney, J. Wang, G. H. Beall, N. F. Borrelli, *Opt. Lett.* **2002**, *27*, 1309.
[31] S. Zhou, H. Dong, H. Zeng, B. Wu, B. Zhu, H. Yang, S. Xu, Z. Wang, J. Qiu, *J. Appl. Phys.* **2007**, *102*, 063106.
[32] Y. Tanabe, S. Sugano, *J. Phys. Soc. Jpn.* **1954**, *9*, 766.
[33] Y. Suzuki, W. A. Sibley, O. H. El Bayoumi, T. M. Roberts, B. Bendow, *Phys. Rev. B* **1987**, *35*, 4472.
[34] S. Zhou, N. Jiang, B. Wu, J. Hao, J. Qiu, *Adv. Funct. Mater.* **2009**, *19*, 2081.
[35] C. J. Ballhausen, *Introduction to Ligand Field Theory*, McGraw-Hill, New York **1962**.
[36] N. F. Mott, R. W. Gurney, *Electronic Processes in Ionic Crystals*, Clarendon, Oxford, UK **1948**.
[37] S. Zhou, G. Feng, B. Wu, N. Jiang, S. Xu, J. Qiu, *J. Phys. Chem. C* **2007**, *111*, 7335.
[38] M. Sharonov, A. Bykov, V. Petricevic, R. Alfano, *Opt. Lett.* **2007**, *32*, 3489.
[39] S. Tanabe, X. Feng, *Appl. Phys. Lett.* **2000**, *77*, 818.
[40] T. C. Brunold, M. F. Hazenkamp, H. U. Güdel, *J. Am. Soc. Soc.* **1995**, *117*, 5598.
[41] M. Hughes, J. E. Aronson, W. S. Brocklesby, D. P. Shepherd, D. W. Hewak, R. J. Curry, *Proc. SPIE* **2004**, *5620*, 289.
[42] H. Sun, F. Shimaoka, M. Fujii, N. Nitta, M. Mizuhata, H. Yasuda, S. Deki, S. Hayashi, *Nanotechnology* **2009**, *20*, 035604.
[43] N. V. Kuleshov, V. G. Shcherbitsky, V. P. Mikhailov, S. Kück, J. Koetke, K. Petermann, G. Huber, *J. Lumin.* **1997**, *71*, 265.
[44] B. Wu, S. Zhou, J. Ruan, Y. Qiao, D. Chen, C. Zhu, J. Qiu, *Opt. Express* **2008**, *16*, 2508.
[45] B. Wu, S. Zhou, J. Ruan, Y. Qiao, D. Chen, C. Zhu, J. Qiu, *Appl. Phys. Lett.* **2008**, *92*, 151102.
[46] A. F. Fercher, W. Drexler, C. K. Hitzenberger, T. Lasser, *Rep. Prog. Phys.* **2003**, *66*, 239.
[47] S. G. Adie, B. W. Graf, A. Ahmad, P. S. Carney, S. A. Boppart, *Proc. Natl. Acad. Sci. USA* **2012**, *109*, 7175.
[48] N. Tessler, V. Medvedev, M. Kazes, S. Kan, U. Banin, *Science* **2002**, *295*, 1506.
[49] A. Jha, S. Shen, M. Naftaly, *Phys. Rev. B* **2000**, *62*, 6215.
[50] S. Zhou, H. Dong, G. Feng, B. Wu, H. Zeng, J. Qiu, *Opt. Express* **2007**, *15*, 5477.
[51] F. Wang, X. Liu, *J. Am. Chem. Soc.* **2008**, *130*, 5642.
[52] S. Zhou, N. Jiang, B. Zhu, H. Yang, S. Ye, G. Lakshminarayana, J. Hao, J. Qiu, *Adv. Funct. Mater.* **2008**, *18*, 1407.
[53] K. Zhang, S. Zhou, Y. Zhuang, R. Yang, J. Qiu, *Opt. Express* **2012**, *20*, 8675.
[54] H. Lin, R. Zhang, D. Chen, Y. Yu, A. Yang, Y. Wang, *J. Mater. Chem. C* **2013**, *1*, 1804.
[55] R. Ceccato, R. Dal Maschio, S. Gialanella, G. Mariotto, M. Montagna, F. Rossi, M. Ferrari, K. E. Lipinska-Kalita, Y. Ohki, *J. Appl. Phys.* **2001**, *90*, 2522.
[56] Y. Xu, X. Zhang, S. Dai, B. Fan, H. Ma, J. Adam, J. Ren, *J. Phys. Chem. C* **2011**, *115*, 13056.